First-passage time approach to kinetic Monte Carlo simulations of metal (100) growth

Giridhar Nandipati,* Yunsic Shim,† and Jacques G. Amar‡
Department of Physics & Astronomy, University of Toledo, Toledo, Ohio 43606, USA
(Received 12 July 2009; revised manuscript received 16 April 2010; published 10 June 2010)

A first-passage-time (FPT) approach to accelerate kinetic Monte Carlo (KMC) simulations of metal(100) epitaxial growth with fast edge diffusion is described. In our approach, the process of singly-bonded edge diffusion is replaced by a calculation of the first-passage time for an edge diffuser to be absorbed either by corner rounding or kink attachment, while the remaining activated processes are treated with regular KMC. To calculate the FPT two different methods were used. In the first more computationally efficient method, the mean FPT was calculated using an analytical expression, which takes into account the difference between the hopping rate for an atom along the edge and at a corner site. In the second method, the full FPT distribution is numerically calculated based on the eigenvectors and eigenvalues of the corresponding transition matrix. As a test of this approach we have studied three different models of multilayer growth, including two irreversible growth models as well as an effective-medium theory model of Cu/Cu(100) growth. By taking into account the interactions of edge diffusers with other atoms we have obtained very good agreement using both methods between our FPT KMC and regular KMC simulations. In addition, we find that our FPT approach can lead to a significant speed-up compared to regular KMC simulations.

DOI: 10.1103/PhysRevB.81.235415 PACS number(s): 68.35.Fx, 05.10.Ln, 81.15.Aa

I. INTRODUCTION

Kinetic Monte Carlo (KMC) is an extremely efficient method[1–6] to carry out nonequilibrium simulations of dynamical processes when the relevant rates are known. As a result, the KMC method has been successfully used to carry out simulations of a wide variety of dynamical processes over experimentally relevant time and length scales. However, in some cases, such as when the relevant processes have a wide range of activation energies, much of the simulation time can be "wasted" on low-barrier repetitive events. As a result, in these cases direct KMC simulations may not be sufficient to reach the time scales of interest.

A variety of approximate approaches to dealing with this "time-scale" problem have been suggested, including the level-set method[7] and other multiscale approaches.[8–11] However, another approach is the use of first-passage-time (FPT) algorithms. In this approach, one avoids simulating the numerous diffusive hops of atoms, and instead replaces them with the first-passage time to make a transition from one "localized basin" to another.[12,13] For example, the FPT method has been used in simulations of annihilating continuum random walkers in two and three dimensions,[14] in Monte Carlo simulations of single-walker propagation,[15,16] as well as to describe dislocation kink nucleation[17,18] and vacancy diffusion in alloys.[19] More recently it has also been demonstrated to be applicable to simulations of radiation damage[20] and vacancy-As cluster dissolution in Si.[21] A slightly different method has also been used to study irreversible submonolayer growth in one-dimensional (1D) extended and two-dimensional (2D) point-island models.[22,23] However, perhaps because of their complexity, FPT techniques have not been previously used to carry out simulations of multilayer epitaxial growth.

Here, we develop and apply a FPT method to accelerate KMC simulations of multilayer epitaxial growth. We note that one of the primary motivations of this work was the observation that, due to the extremely low barrier for edge diffusion in Cu/Cu(100) growth, a great deal of computation time is wasted on repetitive edge-diffusion events even at relatively low temperatures. Accordingly, we have used our method to carry out simulations of a variety of models of epitaxial growth with fast edge-diffusion and a significant barrier for corner rounding. These include a model of Cu/Cu(100) growth with activation barriers based on effective-medium theory (EMT) as well as simpler irreversible growth models including a "generic" model of irreversible fcc(100) growth and a solid-on-solid (SOS) model.

In our simulations, the detailed computation of (one-bond) edge diffusion is replaced by a calculation of the first-passage time for an edge diffuser to be "absorbed," either by attaching to another atom near the edge, or by corner rounding. However, all other KMC events such as deposition, monomer diffusion and detachment are treated using regular KMC. For comparison, we have carried out simulations using both the mean first-passage time (MFPT) as well as the full FPT distribution. In particular, an analytical expression for the MFPT was obtained by combining known expressions for the escape probabilities and mean first-passage-times of a 1D random walker with analytical corrections due to the difference in hopping rate near a corner and along an edge. In contrast, in the case of our simulations using the full FPT distribution, the FPT was numerically obtained by finding the eigenvectors and eigenvalues of the corresponding transition matrix.

Since an edge diffuser can interact with other atoms such as another edge diffuser or a monomer approaching a step, we have also included these interactions in our simulations. While the inclusion of such interactions requires significant overhead, using our FPT method we have been able to achieve a significant speed up in simulations of multilayer epitaxial growth. In addition, we find that there is excellent agreement between our FPT KMC simulations and regular KMC simulations. For completeness, we have also derived explicit expressions for the conditional MFPT.

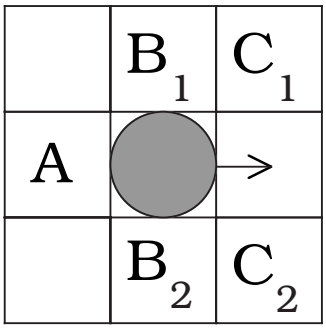

FIG. 1. Diagram showing neighboring sites affecting the energy barrier for intralayer diffusion of a central atom (shaded circle) used in EMT model of Cu/Cu(100) growth [see Eq. (1)].

This paper is organized as follows. In Sec. II, we describe the models used in our simulations. These include an EMT model of Cu/Cu(100) growth as well as two irreversible growth models—a generic model of fcc (100) growth and a SOS model. In Sec. III we describe our FPT approach in detail and also provide the corresponding analytical expressions for the mean first-passage time and absorption probabilities. We also discuss the interactions between an edge diffuser and other atoms as well as the numerical calculation of the FPT distribution. A comparison between simulation results obtained using FPT KMC and regular KMC is then presented in Sec. IV, while a summary of our results is presented in Sec. V. Finally, in Appendix A we derive the corrections to the mean FPT used in Secs. III and IV corresponding to the number of times a diffusing particle hits the boundaries before it is absorbed. Explicit expressions for the conditional FPT are also derived in Appendix B.

II. MODEL

In order to test our FPT KMC method, we have applied it to an EMT model of Cu/Cu(100) growth with fast edge diffusion, which also takes into account the fcc crystalline geometry. We note that this model has previously been used[24,25] to obtain excellent quantitative agreement with the experimental results of Ernst *et al.*[26] for Cu/Cu(100) multilayer growth at 160 and 200 K. More recently it has also been used[27] to explain experimental results for Cu/Cu(100) growth obtained by Botez *et al.*[28]

In this model, the energy barriers for intralayer diffusion correspond to a parameterization of EMT barriers calculated by Jacobsen.[29] In particular, as shown in Fig. 1, in the EMT model the energy barriers for hopping of an adatom on a flat terrace are determined by its interactions with the five neighboring atoms labeled A, B_1, B_2, C_1, and C_2. In particular, if an adatom (filled circle) has a lateral bond with neighboring site i (where $i=A$, B_1, B_2, C_1, and C_2), then the occupation number N_i for that site is 1 and otherwise it is zero. The corresponding energy barrier E_b may then be calculated using the expression,[29]

$$E_b = \frac{E_a}{2} + \frac{E_a}{2}\{\delta(N_A,1) + \delta(N_{C_1},0)\,\delta(N_{C_2},0)\,[1+\delta(N_{B_1},1)\,\delta(N_{B_2},1)]\}, \quad (1)$$

where $E_a=0.425$ eV is the activation energy for monomer diffusion. We note that this expression implies the existence of four possible different values for the intralayer diffusion barrier: $E_a/2$ for atoms without an A neighbor but with one or both of C_1, C_2, E_a for atoms with no neighbors, and also for atoms with an A neighbor and one or both of C_1, C_2, $3E_a/2$ for atoms with an A neighbor and no "B" or "C" neighbors, and $2E_a$ for atoms with an A neighbor and both "B" neighbors and no "C" neighbors.

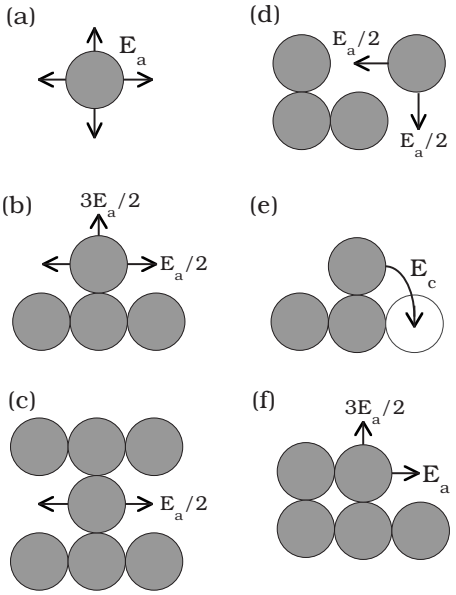

FIG. 2. Diagram showing some important intralayer moves in EMT Cu(100) model along with corresponding activation barriers. (a) monomer diffusion, (b) single-bond edge diffusion and detachment, (c) two-bond edge diffusion, (d) monomer attachment at a step-edge, (e) corner-rounding ($E_c=0.35$ eV), and (f) kink detachment along an edge.

One of the consequences of Eq. (1) is the existence of very "fast" edge diffusion (see Fig. 2) with a barrier ($E_a/2$) which is significantly smaller than that for monomer diffusion. Another consequence is that dimer diffusion (via repetition) is as fast as monomer diffusion. Once the activation barrier is obtained, the rate for a given move is given by $D = D_0 e^{-E_b/k_BT}$ where $D_0=3\times10^{11}$ s^{-1}. We note that this value was determined by comparing the calculated antiphase diffraction factor at a coverage of 0.3 monolayer (ML) at $T=213$ K and deposition rate $F=0.1$ ML/min with the corresponding experimental results of Swan *et al.*[30] In all of our simulations a deposition rate $F=1/120$ ML/s—the same as in the multilayer Cu/Cu(100) growth experiments of Ernst *et al.*[26]—was assumed, while the initial condition corresponded to a flat substrate.

In order to simulate multilayer growth, the model described by Eq. (1) has been modified in two ways.[24] First, to take into account the Ehrlich-Schwoebel (ES) barrier to interlayer diffusion,[31–33] for all interlayer diffusion processes an additional barrier of 0.02 eV is added to the value E_b given by Eq. (1). We note that this should be considered to be an *effective* ES barrier, since both EMT calculations[34] and density-functional theory (DFT) calculations[35] indicate that the ES barrier for interlayer diffusion at a close-packed step edge is significantly higher than at an open step edge. The

second modification involves the barrier for corner rounding [see Fig. 2(e)]. Since Eq. (1) implies that the barrier for an adatom at a corner along a step edge of an island to detach along the edge is given by E_a while the barrier to "reattach" is very small ($E_a/2$), this implies an effective corner-rounding barrier of 0.425 eV. However, in Ref. 24 it was found to be necessary to assume a smaller effective corner-rounding barrier (e.g., $E_c=0.35$ eV) in order to explain the relatively large value of the growth exponent β ($\beta \simeq 1/2$) found in the experiments of Ernst *et al.*[26] at 200 K. Accordingly, in our simulations, this smaller barrier was used. We note that in our model this enhanced corner-rounding move is only allowed to occur for the case of in-plane motion, i.e., no combined enhanced corner-rounding and interlayer diffusion moves are included in our simulations. Finally, we note that in all the results presented here the corner-rounding move was suppressed for dimers and trimers since this leads to enhanced dimer and trimer diffusion.

As in previous simulations of metal(100) growth, also included in our model is downward funneling (DF),[36] for atoms deposited at nonfourfold hollow sites. In KMC simulations with the usual DF and no short-range attraction, atoms are assumed to be deposited only at the underlying fcc(100) lattice sites, each of which corresponds to a "capture zone" for deposition.[37,38] In particular, if a selected deposition site is a fourfold hollow site, then the deposited atom remains where it is immediately after deposition. However, if one or more of the fourfold hollow "support" atoms is missing, then the atom "cascades" randomly to one of the missing support sites. This process is repeated until a fourfold hollow site is found. As in Ref. 24, in the simulations presented here, the deposition process is similar, but with a small modification to take into account the effects of uphill funneling due to short-range (SR) attraction as determined from molecular dynamics simulations.[25] In particular, if an atom lands at a site which is not a fourfold hollow site but for which one or more of the missing support sites are themselves fourfold hollow sites, then one of these fourfold hollow sites is randomly selected. Otherwise, the deposition process is the same as for DF.

Figure 2 shows some of the important intralayer diffusion moves in our EMT model, including monomer diffusion [Fig. 2(a)], singly-bonded edge diffusion with rate $D_e = D_0 e^{-E_a/2k_BT}$ [Fig. 2(b)], double-bond edge diffusion [Fig. 2(c)], corner rounding with rate $D_c = D_0 e^{-E_c/k_BT}$ [Fig. 2(e)], kink detachment [Fig. 2(f)], and kink reattachment [Fig. 2(d)]. As can be seen, the barriers for singly-bonded edge diffusion, doubly-bonded edge diffusion and kink reattachment are very low (e.g., $E_a/2=0.2125$ eV) while the barrier for kink detachment along an edge [see Fig. 2(f)] is the same as for monomer diffusion. Accordingly, we expect that both singly-bonded and doubly-bonded edge diffusion will lead to fast repetitive events which can significantly slow down regular KMC simulations. However, because it turns out that two-bond edge diffusion has almost no effect on either the surface roughness or the surface morphology, and also because the focus here is on applying the FPT method to accelerate single-bond edge diffusion, to save computational time the rate of two-bond edge diffusion has been reduced by a factor of 10 in all of our EMT model simulations. Figure 3 shows all the possible different absorption pathways for a singly bonded edge-diffusing atom in our EMT model along with the corresponding barriers. In addition to (1) kink attachment and (2) corner rounding, these include detachment perpendicular to an edge (3) with or (4) without interlayer diffusion, detachment parallel to an edge (5) with and (6) without interlayer diffusion, and (7) edge diffusion over a step edge. We note that to satisfy detailed balance the reverse barriers for the interlayer diffusion processes 3, 5, and 7 shown in Fig. 3 are all assumed to be equal to $3E_a/2+E_{ES}$.

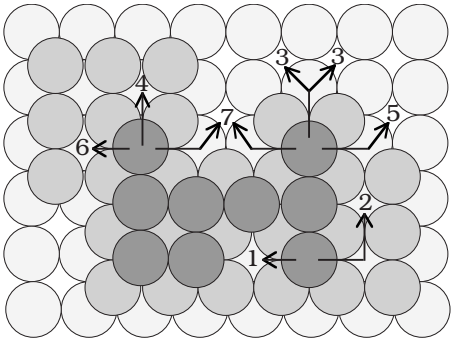

FIG. 3. Pathways for edge and interlayer diffusion in EMT Cu(100) model. Barriers for each process are as follows: (1) $E_a/2$, (2) E_c, (3) $3E_a/2+E_{ES}$, (4) $3E_a/2$, (5) E_a+E_{ES}, (6) E_a, and (7) $E_a/2+E_{ES}$.

In addition to the Cu/Cu(100) growth simulations carried out using the EMT model described above, we have also carried FPT KMC simulations of two simpler irreversible growth models. These include a generic fcc model with DF and irreversible island formation (no detachment) as well as an even simpler solid-on-solid model which is similar to the generic fcc model but which does not take into account the fcc geometry. In order to mimic the effects of DF, in the SOS model any atom deposited at a step edge was assumed to "funnel" down randomly to one of the lower nearest-neighbor sites. For both of these irreversible growth models, the deposition flux, and the rates of monomer interlayer and intralayer diffusion, and corner diffusion were assumed to be the same as for the EMT model.

III. APPLICATION OF FPT METHOD TO KMC

A. Mean number of hops for 1D random walker

Before discussing the application of our FPT method to KMC simulations, we first present the relevant analytical expressions for the mean number of hops $n(x)$ of a 1D random walker (initially at site x) diffusing on the interval $[0,L]$ with partial reflection and absorption at each boundary (see Fig. 4). Away from the boundaries the particle has an equal prob-

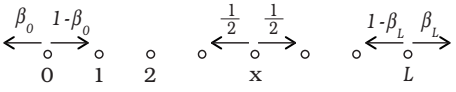

FIG. 4. Schematic showing 1D random walker diffusing between partially absorbing boundaries at 0 and L with absorption probabilities β_0 and β_L, respectively.

ability of moving to the right or to the left at each time step. However, we assume that when the walker arrives at site $0(L)$, it is absorbed with probability $\beta_0(\beta_L)$ and reflected with probability $1-\beta_0(1-\beta_L)$, respectively. The probability $P_0(x,L,\eta_0,\eta_L)$ that a walker initially at site x will be absorbed at 0 is then given by,[39,40]

$$P_0(x,L,\eta_0,\eta_L) = \frac{L-x+\eta_L}{L+\eta_0+\eta_L}, \tag{2}$$

where $\eta_0=(1-\beta_0)/\beta_0$ and $\eta_L=(1-\beta_L)/\beta_L$, while the probability that the walker will be absorbed at site L is given by $P_L(x,L,\eta_0,\eta_L)=1-P_0(x,L,\eta_0,\eta_L)$. In addition, the average number of hops $n(x)$ before a walker initially at site x is absorbed at *either* of the boundaries is given by,[40,41]

$$n(x) = \left[\frac{L(L+2\eta_L)(x+\eta_0)}{(L+\eta_0+\eta_L)} - x^2\right]. \tag{3}$$

While we will primarily make use of Eq. (3) along with additional corrections discussed in Secs. III B 1 and III B 2 to calculate the mean first-passage time, it is also interesting to consider the *conditional* mean number of hops $n_0(x)[n_L(x)]$ corresponding to the average number of hops of a 1D random walker before a particle is absorbed at site $0(L)$. We note that $n_0(x)$ and $n_L(x)$ must satisfy the condition,

$$n(x) = P_0(x,L,\eta_0,\eta_L)n_0(x) + P_L(x,L,\eta_0,\eta_L)n_L(x). \tag{4}$$

We also note that expressions for $n_0(x)$ and $n_L(x)$ were presented in Ref. 40. However, perhaps due to an error in the boundary conditions, these expressions are not correct and do not satisfy Eq. (4). Accordingly, in Appendix B we derive and present correct expressions for the conditional mean number of hops $n_0(x)$ and $n_L(x)$ for a 1D random walker diffusing between two partially absorbing boundaries.

B. Implementation of FPT approach

In our first-passage-time approach, we have replaced the detailed motion of a singly-bonded atom diffusing along an island edge, by a calculation of its overall first-passage time for "absorption" at a kink site or by corner rounding. The remaining diffusive moves in our KMC simulations, for which the barriers are typically significantly higher than for edge diffusion, are treated as regular KMC moves. For simplicity, and also because it is computationally faster, for the two simpler irreversible growth models (SOS model and generic fcc model) we have carried out simulations based on the mean first-passage time, using the analytical expressions discussed below in Secs. III B 1 and III B 2. However, for the case of Cu/Cu(100) growth we have also carried out simulations in which the full FPT distribution $P_a(t)$ for absorption of an edge diffuser at time t is used. We first discuss the analytical expressions corresponding to the mean first-passage time.

1. Analytical calculation of mean FPT

In order to obtain an analytical expression for the mean first-passage time we map the diffusion of an edge-atom to a 1D random walk with partially absorbing boundaries with

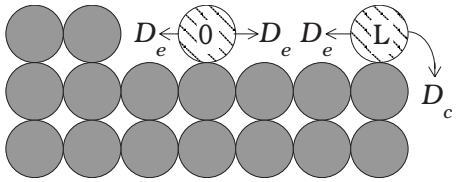

FIG. 5. Example of edge diffusion with two possible absorption pathways: attachment to a kink with rate D_e, and corner rounding with rate D_c.

the appropriate values of x, L, β_0, and β_L. For example, for the case shown in Fig. 5, with kink attachment and corner rounding at the boundaries, one has $x=0$, $L=3$, $\beta_0=1/2$, and $\beta_L=D_c/(D_e+D_c)$ where D_e and D_c are the rates of edge diffusion and corner rounding, respectively. Since the rate for edge hopping in each direction (D_e) is the same for all sites along the edge except for the corner site, the mean first passage time $\tau(x)$ for an edge diffuser at site x to escape from the edge is given by

$$\tau(x) = n(x)/(2D_e) + \Delta t_{av}(x), \tag{5}$$

where $n(x)$ is given by Eq. (3), $1/(2D_e)$ is the average time for each individual hop along the edge, and $\Delta t_{av}(x)$ is a correction term, which takes into account the fact that the total hopping rate at a corner site (D_e+D_c) is different from the rate $(2D_e)$ at all other edge sites. Somewhat surprisingly, this correction turns out to be important to obtain good agreement with regular KMC simulations.

2. Correction term $\Delta t_{av}(x)$

In order to calculate $\Delta t_{av}(x)$, one first needs to calculate the average number of times an edge atom arrives at a corner site before being absorbed. Let us denote by $h_{\alpha_1}(x,\alpha_2)$ the number of times (excluding the last time if $\alpha_1=\alpha_2$) that a walker initially at position x arrives at boundary site α_2 before being absorbed at site α_1 (where $\alpha_1,\alpha_2=0$ or L). Then, assuming that the edge atom was absorbed at boundary site α, the corresponding correction time $\Delta t_\alpha(x)$ to the FPT is given by,

$$\Delta t_\alpha(x) = \delta_0\, h_\alpha(x,0) + \delta_L\, h_\alpha(x,L) + \beta_\alpha/D_\alpha, \tag{6a}$$

$$\delta_\alpha = \frac{\beta_\alpha}{D_\alpha} - \frac{1}{2D_e}, \tag{6b}$$

where δ_α corresponds to the correction time for each hop away from a boundary at site α, D_α is the rate (equal to D_e at a kink and D_c at a corner) for absorption at the boundary, and the last term in Eq. (6a) takes into account the additional time required for the last hop over the boundary. The mean correction time $\Delta t_{av}(x)$ is then obtained by averaging over the possibilities that the edge diffuser is absorbed at site 0 and site L and is given by,

$$\Delta t_{av}(x) = P_0(x)\Delta t_0(x) + P_L(x)\Delta t_L(x), \tag{7}$$

where $P_0(x)$ and $P_L(x)$ are given in Eq. (2) and $\Delta t_0(x)$ and $\Delta t_L(x)$ are given in Eq. (6).

By carrying out an exact enumeration of all possible walks (see Appendix A), we have derived analytical expressions for $h_0(x,0)$, $h_0(x,L)$, $h_L(x,0)$, and $h_L(x,L)$. In particular we find,

$$h_L(x,0) = \frac{\eta_0(\eta_0+1)}{L+\eta_0+\eta_L}\frac{L-x+\eta_L}{x+\eta_0}, \tag{8a}$$

$$h_L(x,L) = \eta_L\left[\frac{L-1+\eta_0}{L+\eta_0+\eta_L}\right]. \tag{8b}$$

The corresponding results for $h_0(x,0)$ and $h_0(x,L)$ may be obtained by interchanging η_0 and η_L and replacing x with $L-x$ in Eqs. (8b) and (8a), respectively.

3. Calculation of FPT distribution $P_a(t)$

Although computationally more demanding, the full FPT distribution $P_a(t)$ for absorption of an edge diffuser at time t may be numerically calculated by considering the master equation,[12,13] for the evolution of the probability $\bar{P}_i(t)$ that the edge diffuser is at site i along the edge, where $i=0,1,2,\ldots,L$. Accordingly one may write,

$$\frac{d\bar{P}}{dt} = -M\bar{P}(t), \tag{9}$$

where the $L+1$ by $L+1$ transition matrix M satisfies $M_{ij}=-R_{j\to i}$ if $i\neq j$ and $M_{ii}=\Sigma_{k\neq i}R_{i\to k}$, and $R_{i\to j}$ is the rate for the edge diffuser to hop from site i to site j. Here the sum over k includes the absorption sites as well as the edge-diffusion sites 0 through L. The solution is,

$$\bar{P}(t) = e^{-Mt}\,\bar{P}(0). \tag{10}$$

Diagonalizing the transition matrix M one may write,

$$\bar{P}(t) = V\,e^{-\Lambda t}\,V^{-1}\bar{P}(0), \tag{11}$$

where $M=V\Lambda V^{-1}$, $\Lambda_{ij}=\lambda_i\delta_{ij}$ is the matrix of eigenvalues, V is the eigenvector matrix, and $\bar{P}(0)$ is the initial probability distribution of the edge diffuser. We can rewrite this as,

$$\bar{P}_i(t) = \sum_j V_{ij}\,e^{-\lambda_j t}\,a_j, \tag{12}$$

where V_{ij} is the ith component of the jth eigenvector and,

$$a_j = \sum_k V^{-1}_{jk}\,\bar{P}_k(0) = V^{-1}_{j,x}, \tag{13}$$

where x is the initial position of the edge diffuser. So the absorption probability at time t is,

$$P_a(t) = 1-\sum_i \bar{P}_i(t) = 1-\sum_{ij} V_{ij}\,V^{-1}_{j,x}\,e^{-\lambda_j t}. \tag{14}$$

Picking an absorption time t with the correct distribution then involves numerically solving the equation,

$$P_a(t) = \xi, \tag{15}$$

where ξ is a uniform random number between 0 and 1. We note that from Eq. (14) an expression for the mean first-passage time τ may also be obtained,

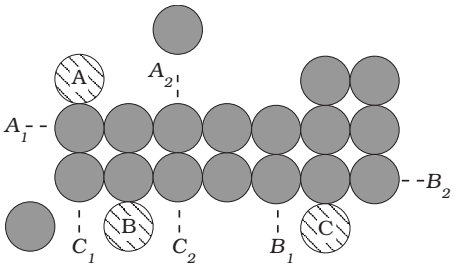

FIG. 6. Examples of edge atoms (striped circles) and their corresponding absorption sites (dashed lines) including interactions with monomers, e.g., absorption sites for atom A are A_1 and A_2.

$$\tau = \int_0^\infty dt\; t\,\frac{dP_a(t)}{dt} = \sum_{ij} V_{ij}V^{-1}_{j,x}/\lambda_j. \tag{16}$$

Thus, both the mean FPT and the FPT distribution $P_a(t)$ may be obtained from the eigenvectors and eigenvalues of the transition matrix M.

We also note that for the models considered here the matrix M is symmetric and, therefore, one may write $V^{-1}=V^T$, which implies that $V^{-1}_{j,x}=V_{x,j}$. In addition, since only edge-diffusion hops to nearest-neighbor sites are allowed the matrix is tridiagonal. Accordingly, the matrix M may be efficiently diagonalized using a method appropriate for tridiagonal, symmetric matrices. In particular, one may write,

$$R_{i\to j} = D_e(\delta_{i,j+1}+\delta_{i,j-1}), \tag{17}$$

for $i,j=0,1,2,\ldots,L$, while $R_{0\to -1}=D_{kc}(0)$ and $R_{L\to L+1}=D_{kc}(L)$ where $D_{kc}(i)=D_e$ if site i is next to a kink site, and $D_{kc}(i)=D_c$ if site i is a corner site.

4. Interactions between edge diffuser and other atoms

While the FPT expressions above give the escape time for an isolated edge diffuser, an edge atom can also interact with other atoms before escaping. Examples include the interaction of an edge atom with another edge atom on the same edge, with another edge atom on a step edge two lattice units away, and with a monomer approaching the same edge either from above or below the step.

We first consider the interaction between an edge atom and another edge atom on the same edge (atoms B and C in Fig. 6). While it is possible to use the numerical method described in Sec. III B 3 to obtain the distribution of collision times and collision locations for two edge diffusers along an edge, such a calculation is very computationally demanding since it involves finding the eigenvalues and eigenvectors of an $L(L+1)$ by $L(L+1)$ matrix, and also selecting from L collision sites with the appropriate probability. Therefore, in order to approximately include such an interaction in our simulations, for each edge diffuser we have treated any neighboring edge diffuser as a stationary kink site (see sites C_2 and B_1 in Fig. 6). However, to take into account the fact that the relative diffusion rate is twice the rate of a single edge diffuser, the calculated FPT for collision of each edge diffuser with the other is divided by a factor of 2.

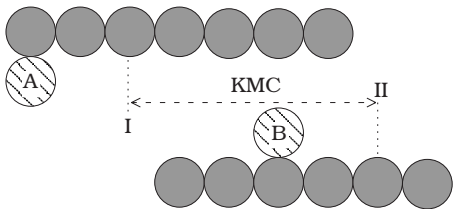

FIG. 7. Two interacting step edges. Edge atoms between sites I and II are treated with regular KMC, while edge atoms outside this region (e.g., atom A) are treated using FPT KMC.

Similarly, if at time t a monomer approaches a step edge on the lower terrace one step away from the step edge, then the monomer may also be treated as a kink site (Fig. 6, sites A_2 and C_1). However, before doing so the edge diffuser should first be moved, with the appropriate probability distribution $\bar{P}_i(t)$ to one of the sites i along the edge. While it is in principle possible to calculate $\bar{P}_i(t)$ for all sites along the edge, and then to use this distribution to move the edge diffuser to one of the edge sites with the appropriate probability, such a calculation is at least as computationally demanding as the calculation of $P_a(t)$. In addition, since the rate of edge diffusion is significantly higher than the monomer hopping rate as well as the (per site) deposition rate, it is a reasonable approximation to assume that the edge diffuser is equilibrated along the step edge. Accordingly, in this case the edge diffuser is first moved to a random site along the edge before calculating the FPT to attach to the monomer. For the SOS model this equilibration is particularly important if the monomer arrives from the upper step. In this case the edge diffuser is first moved to a random site along the edge before either performing interlayer diffusion or calculating the effective DF due to knockout for a freshly deposited atom at a step edge. We note that while the inclusion of such approximate equilibration processes only affects the surface roughness very weakly, it has a strong effect on the surface morphology, and is therefore important to include especially in SOS models.

Finally, we consider the interaction between two edge diffusers, which are on edges which are two steps away as shown in Fig. 7. In this case, regular KMC is used when both edge atoms are in the common region (in between I and II) as shown in Fig. 7. Including this process is particularly important in order to properly include island coalescence in our simulations. Otherwise, FPT KMC is used with sites I and II treated as kink sites.

In order to take these interactions into account we associate each lattice site with a list of edge diffusers it can affect. Accordingly, every time there is a change at the site all affected edge diffusers are updated. We note that all sites one step away from the edge as well as both absorption sites are linked with the edge diffuser in this way. In the case of the EMT model, all potential edge diffuser support sites one step away from the edge (see Fig. 8) are also linked with the edge diffusing atom in order to properly take into account the effects of steps on absorption.

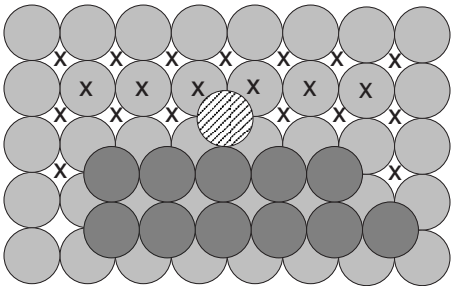

FIG. 8. Schematic showing possible interaction sites (marked with x) associated with edge diffuser (striped circle).

5. Time-based KMC

In order to implement our FPT approach we have used a time-based rather than a rate-based method. Thus, in addition to maintaining a list of first-passage times for all edge diffusers, after each event we also update the total rate for all regular KMC moves $R_{\mathrm{KMC}}=\Sigma n_i R_i$ (where R_i is the rate for a process of type i, and n_i is the number of processes of this type). This rate is then used to calculate the time before the next regular KMC event given by $\Delta t_{\mathrm{KMC}}=-\ln(\xi)/R_{\mathrm{KMC}}$, where ξ is a uniform random number between 0 and 1. This time is then compared with the time of the earliest FPT event (selected using another binary tree). If the event type corresponds to a regular KMC event, then the specific event is selected randomly from one of the possible events of this type. [We note that for the Cu/Cu(100) growth model there are 8 possible barriers and/or event types corresponding to a binary tree of order 3.] After each event the lists containing the number and location of all regular KMC processes of each type are updated along with any changes to the neighborhood (e.g., absorption sites, length of the edge, and type of boundaries) of all FPT atoms. We note that in the case of an FPT move, Eq. (2) is used to determine to which absorption site the edge diffuser will escape.

IV. RESULTS

We first consider the application of our FPT KMC method to the irreversible fcc(100) and SOS growth models described in Sec. II We note that for these models all of the FPT results shown are based on the MFPT calculated using Eq. (5) rather than the full FPT distribution. In all of our simulations, we start with a flat substrate (system size $L=256$) and atoms are deposited randomly at an average deposition rate $F=1/120$ ML/s, while the rates for monomer interlayer and intralayer diffusion, and corner rounding were assumed to be the same as for the EMT model at the corresponding temperature. However, since these simulations were considerably slower than those for the corresponding EMT Cu/Cu(100) growth model, a somewhat lower edge-diffusion rate was assumed for the irreversible growth model simulations. In particular, in both the regular KMC and MFPT KMC simulations the edge-diffusion rate in the SOS model [fcc(100) model] simulations was reduced by a factor of 10 (100) compared to the EMT Cu/Cu(100) growth model (see Table I). All of our results were averaged over 10 runs.

TABLE I. Parameters used for irreversible growth model simulations. Here D is the total rate for monomer diffusion, while D_e, D_c, and D_{ES} are the rates for edge diffusion, corner diffusion, and interlayer diffusion, respectively.

Temperature (K)	D/F	D_e/F	D_c/F	D_{ES}/F
fcc(100) 200	7.0×10^2	1.6×10^6	5.5×10^4	2.2×10^2
fcc(100) 250	9.7×10^4	1.9×10^7	3.2×10^6	3.9×10^4
SOS 200	7.0×10^2	1.6×10^7	5.5×10^4	2.2×10^2
SOS 250	9.7×10^4	1.9×10^8	3.2×10^6	3.9×10^4

Figure 9 shows a comparison between regular KMC and MFPT KMC results for the surface roughness or "width" (e.g., rms height fluctuation) as a function of film thickness for both models at $T=200$ and 250 K. As can be seen, there is excellent agreement between the KMC and MFPT simulation results. Similar good agreement (not shown) has also been obtained for the lateral correlation length r_c (corresponding to the first zero crossing of the circularly averaged height-height correlation function) as well as for the circularly averaged height-height correlation function $G(r)$. A comparison between the corresponding morphologies obtained from KMC and MFPT simulations at $T=200$ K for both models is also shown in Fig. 10. As can be seen, there is also good agreement between the morphology obtained from our MFPT simulations and that obtained in regular KMC simulations.

We now consider the speed-up of our MFPT simulations compared to regular KMC simulations. As can be seen in Table II, for the fcc model the MFPT simulations at 200 K

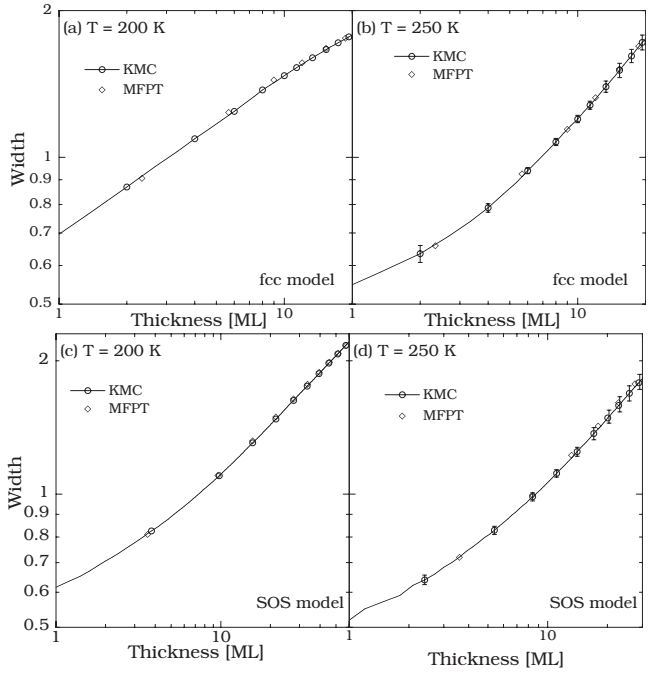

FIG. 9. Comparison of regular KMC results (symbols) and MFPT KMC results (lines) for surface roughness obtained from simulations of irreversible growth models at 200 and 250 K. (error bars for 200 K are of the size of circles).

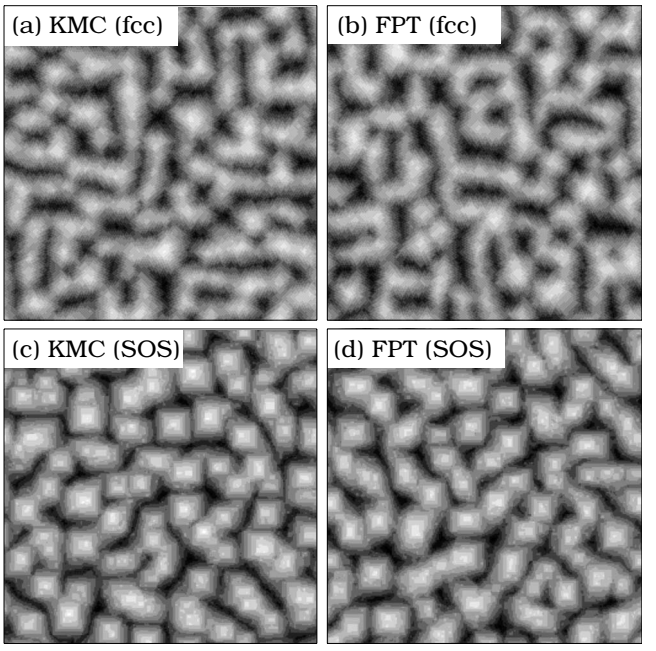

FIG. 10. Comparison of surface morphology ($L=256$) at $T=200$ K obtained in (a) regular KMC and (b) MFPT KMC simulations of generic fcc model at coverage of 20 ML and (c) regular KMC and (d) MFPT KMC simulations of SOS model at 30 ML.

are approximately 63 times faster than the corresponding KMC simulations. In addition, since the rate of edge diffusion increases with temperature, at 250 K the speed-up factor (100) is even larger. However, partly due to the fact that the rate of corner diffusion also increases with increasing temperature, the increase in the speed-up factor from 200 to 250 K is not as large as the increase in the rate of edge diffusion.

Similar results for the SOS model are also shown in Table II. However, perhaps in part because of the simplicity of the SOS model (which leads to reduced overhead for regular KMC) the speed-up factors for the SOS model are not quite as large as for the generic fcc growth model. In particular, for the SOS model the MFPT KMC simulations at 200 K (250 K) are approximately 36 (76) times faster than the corresponding regular KMC simulations. However, the speed up increases significantly with increasing temperature.

We now consider the application of our FPT KMC method to simulations of Cu/Cu(100) growth using our EMT model. In this case we have carried out both FPT KMC simulations using the full FPT distribution [see Eq. (15)] as well as MFPT simulations using the mean FPT calculated

TABLE II. Speed-up factors (compared to regular KMC) obtained in MFPT (FPT distribution) KMC simulations of multilayer growth at $T=200$ and 250 K using different models with Cu parameters.

Model	200 K	250 K
fcc	63	100
SOS	36	76
EMT	42 (28)	31 (22)

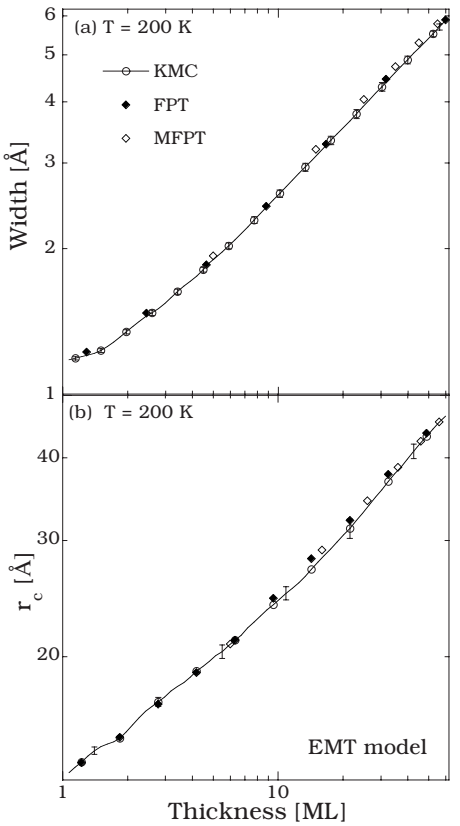

FIG. 11. Comparison of regular KMC (open circles) and MFPT KMC (open diamonds) and FPT distribution (filled diamonds) results for surface roughness and lateral correlation length (r_c) obtained in simulations using EMT model of Cu/Cu(100) growth at 200 K.

using Eq. (5). We first consider growth at 200 K, since at this temperature there is negligible one-bond and two-bond detachment. Representative error bars are shown in Fig. 11 for the regular KMC simulations while all results are averaged over 10 runs. As can be seen in Fig. 11(a), there is very good agreement between the MFPT KMC results (filled symbols) and regular KMC results (open circles, line) for the surface roughness. Similarly good agreement is also shown between the results obtained using the full FPT distribution and the regular KMC results. As shown in Fig. 11(b), similarly good

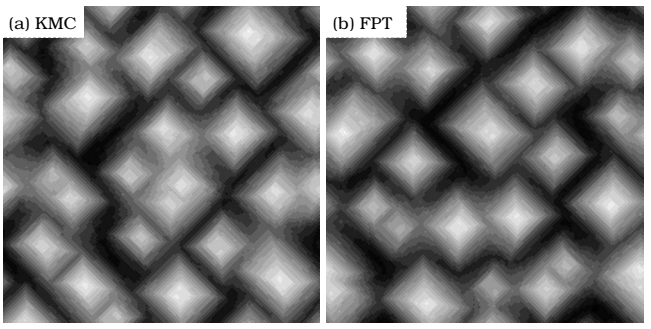

FIG. 12. Comparison of surface morphology (L=256) obtained in regular (a) KMC and (b) FPT distribution KMC simulations of EMT model of Cu/Cu(100) growth at coverage of 60 ML.

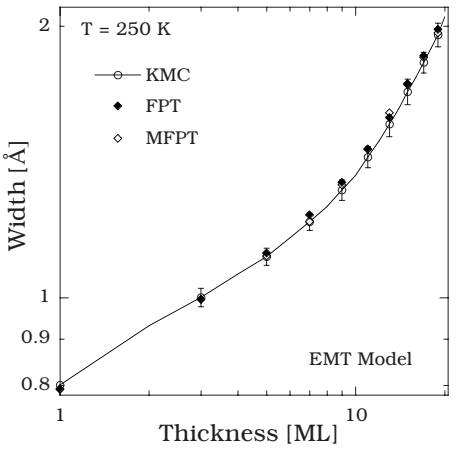

FIG. 13. Comparison of regular KMC (open circles) and MFPT KMC (open diamonds) and FPT distribution (filled diamonds) results for surface roughness obtained in simulations using EMT model of Cu/Cu(100) growth at 250 K.

agreement has also been obtained for the lateral correlation length. As indicated by Figs. 12(a) and 12(b), there is also very good agreement between the morphology obtained using FPT KMC and that obtained using regular KMC.

We note that at 200 K the regular KMC simulations are quite time-consuming and take approximately 4 days for each 60 ML run. However, our FPT simulations are significantly faster. In particular, as shown in Table II using the MFPT we obtain a speed up of approximately 42 over regular KMC simulations, while a smaller speed-up factor is obtained in our simulations using the full FPT distribution, due to the additional overhead required in this case.[42] We note that in this case we have saved the eigenvalues and eigenvectors for each value of the initial position x and edge-length L so that they do not need to be recalculated if the same configuration is encountered. For comparison we have also carried out MFPT simulations at 200 K with two-bond edge diffusion completely suppressed. While this has little effect on the surface morphology, in this case the speed up due to the use of the FPT is even larger (approximately 65).

Finally, we consider our EMT model of Cu/Cu(100) growth at 250 K. As can be seen in Fig. 13 there is very good agreement between our FPT KMC simulations and regular KMC simulations. In addition, our FPT simulations are again significantly faster than regular KMC simulations. However, due to the increased rates of double-bond edge diffusion and corner rounding at this temperature, in this case the speed-up factors for MFPT and FPT distribution simulations (see Table II) are not quite as large as at 200 K. As an additional test, we have also carried out MFPT simulations of Cu/Cu(100) growth at this temperature using a slightly higher value for the barrier for corner rounding (e.g., using the EMT value E_c=0.425 eV for corner detachment rather than enhanced corner rounding). In this case, due to the higher barrier for corner rounding the speed-up factor increased from approximately 30 to 43.

V. DISCUSSION

Motivated by the observation that in KMC simulations of growth models with fast edge diffusion, a great deal of computer time is wasted on repetitive edge-diffusion events, we have developed a FPT method for accelerating KMC simulations. In our method, the detailed computation of edge-diffusion events is replaced by a calculation of the first-passage time for an edge diffuser to be absorbed, either by attaching to another atom near the edge, or by corner rounding. However, all other KMC events such as deposition, monomer diffusion, and detachment are treated using regular KMC.

For comparison, we have carried out simulations using both the MFPT as well as the full FPT distribution. In particular, an analytical expression for the MFPT [Eq. (5)] was obtained by combining known expressions for the escape probabilities and mean first-passage times of a 1D random walker, with analytical corrections due to the difference in hopping rate near a corner and along an edge. In contrast, in our FPT simulations, the full FPT distribution $P_a(t)$ was numerically obtained by finding the eigenvectors and eigenvalues of the corresponding transition matrix. A first-passage time with the correct distribution was then generated by numerically solving the equation $P_a(t)=\xi$ where ξ is a uniform random number between 0 and 1.

By using these expressions and also taking into account the interactions between an edge diffuser and other atoms, we have obtained excellent agreement between our FPT KMC simulations and regular KMC simulations for a variety of different growth models. These include an EMT model of Cu/Cu(100) growth as well as simpler models of irreversible growth including a generic fcc model and an SOS model. In addition, despite the additional computational overhead required to keep track of the interactions between an edge diffuser and other atoms, we have found a significant speed up in our FPT KMC simulations compared to regular KMC simulations. For example, in our MFPT simulations of Cu/Cu(100) growth at 200 and 250 K, we have obtained speed-up factors of 42 and 31, respectively. We note that the decrease in the acceleration factor as the temperature is increased from 200 to 250 K is due in part to the increase in both the rate of corner rounding and kink detachment with increasing temperature.

In MFPT KMC simulations of a generic fcc model with the same parameters for monomer diffusion, edge diffusion, corner rounding, and interlayer diffusion as in our EMT model, we have obtained even larger speed-up factors (e.g., 63 at 200 K and 100 at 250 K). Similar speed-up factors have also been obtained for the corresponding SOS model at 200 and 250 K. The larger acceleration obtained for these models is in part due to the fact that compared to the EMT model, in these models edge-diffusion plays an even more dominant role. Similarly, the increase in the FPT acceleration factor with increasing temperature is due to the increase in the rate of edge diffusion. However, the barrier for corner rounding also plays an important role. For example, in MFPT KMC simulations of our EMT model at $T=250$ K using the EMT value of the barrier for corner rounding (rather than enhanced corner rounding) the speed-up factor increased from 31 to 43.

Interestingly, our results suggest that (at least for the models studied here) the more computationally efficient MFPT method is as accurate as using the full FPT distribution. In addition, we found that our simulations using the full FPT distribution (without saving the eigenvectors and eigenvalues) were approximately 40% slower than the MFPT simulations although they were somewhat faster (see Table II) when the eigenvectors and eigenvalues were saved. However, despite these disadvantages the numerical method to calculate the full FPT distribution has a number of other advantages. In particular, it can be easily applied to study more complicated cases, such as those with longer-range interactions or in which the hopping rate of an edge diffuser depends on its position along the edge.

In addition to deriving expressions for the appropriate absorption probabilities and mean first-passage time as discussed in Sec. III B 2, we have also derived expressions for the conditional MFPT (see Appendix B). However, we found that our conditional MFPT KMC simulations are several times slower than the corresponding MFPT KMC simulations, due at least in part to the more complicated expressions required to calculate the conditional FPT. Accordingly, here we have focused on FPT KMC simulations and have not presented any conditional FPT KMC results.

We note that the inclusion of interactions between an edge diffuser and other atoms turns out to be crucial in using our FPT method to obtain accurate results. This includes the interaction with other edge diffusers on the step edge or a nearby step edge, and with monomers approaching the step edge from above and below. In particular, the interaction with another edge diffuser was included by treating the other edge diffuser as a kink atom and dividing the FPT by a factor of 2 to take into account the relative motion of both edge diffusers. We have also assumed that by the time another atom approaches a step edge on which there is already an edge diffuser, this edge diffuser is already equilibrated. This is done by randomly relocating the edge-diffuser along the edge before recalculating the corresponding FPT. While this equilibration assumption does not strongly affect the surface roughness, it turns out to be crucial in obtaining good agreement with the surface morphology observed in regular KMC simulations.

Since the FPT method requires significant overhead, in both our KMC and FPT KMC simulations we have taken care to maximize the efficiency. For example, in both cases binary trees were used to select the next event. In addition, in both KMC and FPT KMC simulations the regular KMC events were organized into lists of different types in order to minimize the size of the corresponding binary tree. Nevertheless, significant additional overhead was still required in our FPT KMC simulations to keep track of the interactions between an edge diffuser and other atoms. If in the future a more efficient method is devised to take these interactions into account then this could significantly increase the speed-up possible via FPT KMC simulations.

Since the implementation of our FPT KMC method is also relatively complex, it is of interest to compare it with simpler although perhaps less accurate methods. For example, one possible method to accelerate simulations with fast repetitive events, is to artificially reduce the rate of these events by a

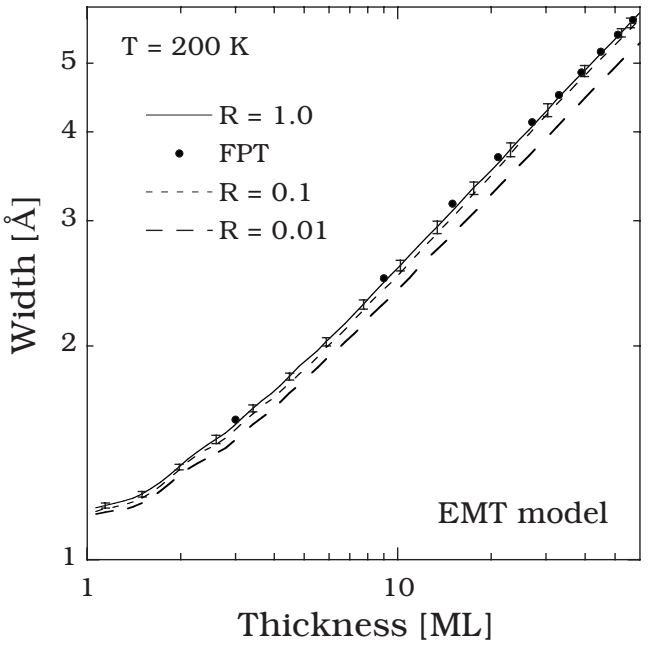

FIG. 14. Dependence of surface roughness on edge-reduction factor R obtained in regular KMC simulations of EMT model of Cu/Cu(100) growth at 200 K.

factor of R where $R<1$. However, while this can lead to a speed up of up to a factor of $1/R$, care must still be taken to ensure that detailed balance is maintained. For the models considered here which have a relatively short range of interaction, this can be done by using edge reduction, i.e., reducing the rate of edge diffusion for all singly bonded edge diffusers, which are more than one hop away from a kink or other attachment site.

Figure 14 shows a comparison between the results of regular KMC simulations using the EMT model at $T=200$ K and KMC simulations carried out using different edge-reduction factors ranging from $R=1.0$ (no reduction) to $R=0.01$. Also shown for comparison are results obtained using the full FPT distribution. As can be seen, while there is good agreement between the KMC and FPT KMC simulations, the results obtained with $R=0.1$ and 0.01 deviate significantly from the KMC results at large thicknesses. In addition, the FPT KMC simulations are approximately 6 times faster than the edge-reduction simulations with $R=0.1$ and are also as fast as the edge-reduction simulations with $R=0.01$. Thus our FPT KMC method provides a more accurate and efficient way to accelerate KMC simulations with fast edge diffusion.

Finally, we discuss some possible improvements to our FPT KMC simulations. As already noted, in the case of an edge-diffuser interacting with an atom approaching a step edge, we have made the approximation that the edge diffuser is completely equilibrated by the time the interacting atom approaches. However, using the transition matrix it is possible to exactly select the position of the edge diffuser with the appropriate probability distribution before determining the FPT with this interaction included. Similarly, in the case of two edge diffusers on the same edge, we have used the approximation of treating each one as a kink site for the other. In this case, the corresponding $L(L+1)$ by $L(L+1)$ transition matrix could also be used to calculate the first-passage-time distribution for two edge diffusers to collide, along with the corresponding probability distribution for the point of collision. However, this is likely to require significant overhead, especially for large values of L. In the future, it would be interesting to determine to what extent the additional computational overhead associated with these more exact calculations reduces the overall computational speed up compared to the results presented here.

ACKNOWLEDGMENTS

This work was supported by the NSF through Grants No. CCF-0428826, No. DMR-0606307, and No. DMR-0907399. We would also like to acknowledge grants of computer time from the Ohio Supercomputer Center (Grant No. PJS0245).

APPENDIX A: DERIVATION OF EQ. (8)

Consider a random walk on the interval $[0,L]$ with partially absorbing boundaries (see Fig. 4). β_0 and β_L are the absorption probabilities at the boundary sites while $\eta_0=(1-\beta_0)/\beta_0$ and $\eta_L=(1-\beta_L)/\beta_L$. We first consider the quantity $h_L(x,L)$ [see Eq. (8b)] corresponding to the number of times (excluding the last time) the walker reaches the right boundary at L before it is absorbed at the right boundary. To simplify our notation we define the quantity $Q_L(x)=P_L(x,L-1,\eta_0,1)$ [see Eq. (2)] corresponding to the probability that a particle initially at x reaches site L at least once. Similarly, $Q_L(L-1)=P_L(L-1,L-1,\eta_0,1)$ is the probability that a particle initially at $L-1$ reaches site L at least once. One may then write,

$$h_L(x,L)=\frac{\sum_{n=1}^{\infty} nQ_L(x)[Q_L(L-1)(1-\beta_L)]^{n-1}\beta_L}{\sum_{n=1}^{\infty} Q_L(x)[Q_L(L-1)(1-\beta_L)]^{n-1}\beta_L}-1. \tag{A1}$$

Here, the factor of $Q_L(x)$ in each sum corresponds to the probability that the particle reaches L the first time, while the expression with exponent $n-1$ corresponds to the probability that it is reflected from L and then returns to L, $n-1$ times. The factor of β_L in each sum corresponds to the probability that it is absorbed at L the last time, while 1 is subtracted since the last time is excluded. Using Eq. (2) one obtains, $Q_L(x)=P_L(x,L-1,\eta_0,1)=\frac{x+\eta_0}{L+\eta_L}$ and $Q_L(L-1)=P_L(L-1,L-1,\eta_0,1)=\frac{L-1+\eta_0}{L+\eta_L}$. Substituting and using the formula for an infinite geometric series leads to Eq. (8b).

Next, we consider the quantity $h_L(x,0)$ [see Eq. (8a)] corresponding to the number of times the walker reaches the left boundary at 0 before it is absorbed at the right boundary. In this case one may write,

$$h_L(x,0) = \frac{Q_0(x)(1-\beta_0)[1-Q_0(1)]\sum_{n=1}^{\infty} n[Q_0(1)(1-\beta_0)]^{n-1}}{1-Q_0(x)+Q_0(x)(1-\beta_0)[1-Q_0(1)]\sum_{n=1}^{\infty}[Q_0(1)(1-\beta_0)]^{n-1}}, \tag{A2}$$

where $Q_0(x)=P_0(x-1,L-1,1,\eta_L)$ is the probability that a walker initially at site x will reach site 0 at least once. Here, the factor of $Q_0(x)$ in the numerator corresponds to the probability that a walker initially at site x will reach site 0 at least once while the factors of $1-\beta_0$ correspond to the probability that it is reflected every time. The factors of $Q_0(1)$ in the summation correspond to the probability that the walker reaches the left boundary after being reflected from site 0, while the extra factor of $1-Q_0(1)$ corresponds to the probability that after $n-1$ reflections the walker is absorbed at the right boundary. The denominator is similar except for the absence of a weighting factor of n, as well as an additional $1-Q_0(x)$ term corresponding to the probability that the walker does not reach the left boundary even once. Using Eq. (2) one obtains, $Q_0(x)=P_0(x-1,L-1,1,\eta_L)=\frac{L-x+\eta_L}{L+\eta_L}$ and $Q_0(1)=P_0(0,L-1,1,\eta_L)=\frac{L-1+\eta_L}{L+\eta_L}$. Substituting and using the formula for an infinite geometric series leads to Eq. (8a).

APPENDIX B: CONDITIONAL FIRST-PASSAGE TIMES

While we have used Eq. (3) for the *unconditional* mean FPT $n(x)$ for a random walker initially at site x to be absorbed at *either* boundary in our FPT KMC simulations, it is also interesting to consider the *conditional* first-passage time (CFPT) corresponding to the average number of hops before a particle is absorbed at a *specific* boundary, i.e., $n_0(x)[n_L(x)]$ corresponding to the average number of hops before a particle is absorbed at site $0(L)$. As mentioned in Sec. III A, the CFPT expressions for a 1D random walker derived in Ref. 40 do not satisfy the probability conservation condition Eq. (4) due to an error in the boundary conditions. Here, we present an outline of the derivation using the correct boundary conditions.

We first define the quantities $m_0(x)=P_0(x,L,\eta_0,\eta_L)n_0(x)$ and $m_L(x)=P_L(x,L,\eta_0,\eta_L)n_L(x)$ which satisfy the recursive relation,

$$\frac{1}{2}m_0(x+1)-m_0(x)+\frac{1}{2}m_0(x-1)=-P_0(x,L,\eta_0,\eta_L), \tag{B1}$$

with boundary conditions,

$$m_0(1)=\frac{1}{1-\beta_0}m_0(0)-P_0(0,L,\eta_0,\eta_L) \tag{B2}$$

$$m_0(L-1)=\frac{1}{1-\beta_L}m_0(L)-P_0(L,L,\eta_0,\eta_L). \tag{B3}$$

Solving Eqs. (B1)–(B3) recursively, we get a unique expression for $m_0(x)$. Dividing by $P_0(x,L,\eta_0,\eta_L)$ we obtain,

$$n_0(x)=\frac{1}{3(L+x+\eta_L)}\left\{x[x^2-3(L+\eta_L)x-1]+\frac{(x+\eta_0)\psi(\eta_L)}{(L+\eta_o+\eta_L)}\right\}, \tag{B4}$$

where $\psi(\eta)\equiv(L+2\eta)(L^2+3\eta L-1)+(L+\eta)(L^2+2)$. Replacing x by $L-x$ in Eq. (B4) and interchanging η_0 and η_L an expression for $n_L(x)$ may also be obtained,

$$n_L(x)=\frac{1}{3(x+\eta_0)}\left\{(L-x)[(L-x)^2-3(L+\eta_0)(L-x)-1]+\frac{(L-x+\eta_L)\psi(\eta_0)}{(L+\eta_0+\eta_L)}\right\}. \tag{B5}$$

We note that these expressions satisfy the probability conservation condition Eq. (4).

*gnandip@physics.utoledo.edu
†yshim@physics.utoledo.edu
‡jamar@physics.utoledo.edu

[1] A. B. Bortz, M. H. Kalos, and J. L. Lebowitz, J. Comput. Phys. **17**, 10 (1975).
[2] G. H. Gilmer, J. Cryst. Growth **36**, 15 (1976).
[3] A. F. Voter, Phys. Rev. B **34**, 6819 (1986).
[4] P. A. Maksym, Semicond. Sci. Technol. **3**, 594 (1988).
[5] K. A. Fichthorn and W. H. Weinberg, J. Chem. Phys. **95**, 1090 (1991).
[6] J. L. Blue, I. Beichl, and F. Sullivan, Phys. Rev. E **51**, R867 (1995).
[7] M. F. Gyure, C. Ratsch, B. Merriman, R. E. Caflisch, S. Osher, J. J. Zinck, and D. D. Vvedensky, Phys. Rev. E **58**, R6927 (1998).
[8] C. A. Haselwandter and D. D. Vvedensky, Phys. Rev. Lett. **98**, 046102 (2007).
[9] C. C. Chou and M. L. Falk, J. Comput. Phys. **217**, 519 (2006).
[10] J. P. DeVita, L. M. Sander, and P. Smereka, Phys. Rev. B **72**, 205421 (2005).

[11] C. C. Fu, J. D. Torre, F. Willaime, J. L. Bocquet, and A. Barbu, Nature Mater. **4**, 68 (2005).
[12] M. A. Novotny, Phys. Rev. Lett. **74**, 1 (1995).
[13] D. T. Gillespie, *Markov Processes: An Introduction for Physical Scientists* (Academic Press, New York, 1992).
[14] T. Opplestrup, V. V. Bulatov, G. H. Gilmer, M. H. Kalos, and B. Sadigh, Phys. Rev. Lett. **97**, 230602 (2006).
[15] M. Mascagni and N. A. Simonov, SIAM J. Sci. Comput. (USA) **26**, 339 (2004).
[16] J. A. Given, J. B. Hubbard, and J. F. Douglas, J. Chem. Phys. **106**, 3761 (1997).
[17] C. S. Deo and D. J. Srolovitz, Modell. Simul. Mater. Sci. Eng. **10**, 581 (2002).
[18] W. Cai, M. H. Kalos, M. de Koning, and V. V. Bulatov, Phys. Rev. E **66**, 046703 (2002).
[19] D. R. Mason, R. E. Rudd, and A. P. Sutton, Comput. Phys. Commun. **160**, 140 (2004).
[20] A. Donev, V. V. Bulatov, T. Oppelstrup, G. H. Gilmer, B. Sadigha, and M. H. Kalos, J. Comput. Phys. **229**, 3214 (2010).
[21] B. Puchala, M. L. Falk, and K. Garikipati, J. Chem. Phys. **132**, 134104 (2010).
[22] V. I. Tokar and H. Dreyssé, Phys. Rev. E **77**, 066705 (2008).
[23] V. I. Tokar and H. Dreyssé, Phys. Rev. B **80**, 161403(R) (2009).
[24] Y. Shim and J. G. Amar, Phys. Rev. B **73**, 035423 (2006).
[25] J. Yu and J. G. Amar, Phys. Rev. Lett. **89**, 286103 (2002).
[26] H.-J. Ernst, F. Fabre, R. Folkerts, and J. Lapujoulade, Phys. Rev. Lett. **72**, 112 (1994).
[27] V. Borovikov, Y. Shim, and J. G. Amar, Phys. Rev. B **76**, 241401(R) (2007).
[28] C. E. Botez, W. C. Elliott, P. F. Miceli, and P. W. Stephens, Phys. Rev. B **66**, 075418 (2002).
[29] T. Einstein, J. Jacobsen, and C. Schiff, Bull. Am. Phys. Soc. **42**, 26 (1997).
[30] A. K. Swan, Z.-P. Shi, J. F. Wendelken, and Z. Zhang, Surf. Sci. **391**, L1205 (1997).
[31] The ES barrier typically refers to the difference (for otherwise equivalent processes) between the barrier in the case of interlayer diffusion and in the case of intralayer diffusion.
[32] G. Ehrlich and F. G. Hudda, J. Chem. Phys. **44**, 1039 (1966).
[33] R. L. Schwoebel, J. Appl. Phys. **40**, 614 (1969).
[34] J. Merikoski, I. Vattulainen, J. Heinonen, and T. Ala-Nissila, Surf. Sci. **387**, 167 (1997).
[35] G. Boisvert and L. J. Lewis, Phys. Rev. B **56**, 7643 (1997).
[36] J. W. Evans, D. E. Sanders, P. A. Thiel, and A. E. DePristo, Phys. Rev. B **41**, 5410 (1990).
[37] M. C. Bartelt and J. W. Evans, Phys. Rev. Lett. **75**, 4250 (1995).
[38] J. G. Amar and F. Family, Phys. Rev. B **54**, 14742 (1996).
[39] J. G. Amar and F. Family, Phys. Rev. Lett. **77**, 4584 (1996).
[40] A. El-shehawey, J. Phys. A **33**, 9005 (2000).
[41] S. Redner, *A Guide to First-Passage Processes* (Cambridge University Press, New York, 2001).
[42] In particular, while a regular KMC simulation of our EMT model of Cu/Cu(100) growth at $T=200$ K (60 ML, $L=256$) takes approximately 4 days on the Ohio Supercomputer Center (OSC)'s Glenn cluster, the corresponding MFPT KMC simulation takes only 2.3 h.